MOTIVECTION
Journal of Mechanical Electrical and Industrial Engineering

Volume : 5, Number : 3, 2023
ISSN : 2655 – 7215 [printed] ; 2685-2098 [online]
DOI : 10.46574/motivection.v5i3.247

Design of Remote Monitoring Application on Non-Rechargeable Battery Redundant System

Wahyudi Purnomo[1], Wahyu Adhie Candra[1], Gabriel Muhammad Manuel[1]*

Abstract

In this era of continuously evolving technology, remote monitoring has emerged as an innovative and effective solution for monitoring and managing remote areas. Design of Remote Monitoring on Non-Rechargeable Battery Redundant System proposes an improved system for multi-point to point remote monitoring, battery redundant, and communication. The study investigated the accuracy of INA219 sensor readings on the battery, the Quality of Service (QoS) of the Message Queuing Telemetry Transport (MQTT) communication protocol from multiple devices based on the TIPHON standard, and the utilization of a High-Side Bootstrap circuit for the battery redundant system. The results indicate that the INA219 sensor shows an average error of 0.64% - 1.04% for voltage and 1.17% - 2.45% for current. Quality of Service testing revealed an average delay of 40.9 - 119.7 ms with 0% packet loss, thus meeting the excellent standard. Bootstrap High-Side circuit efficiency average from all devices are 99.35% for input and 95.9% for output. Lastly, the redundant system by utilizing Bootstrap High-Side circuit achieved a 100% success rate for all devices, confirming the successful design implementation.

Keywords
Remote Monitoring, MQTT, Quality of Service, High-Side Bootstrap, Battery Redundant System

[1] *Department of Manufacturing Automation and Mechatronics Engineering,*
Bandung Polytechnic for Manufacturing
Jl. Kanayakan No.21, Dago, Kecamatan Coblong, Kota Bandung, Jawa Barat 40135

* gamma.gabriel.m@gmail.com

Submitted : May 30, 2023. Accepted : July 13, 2023. Published : July 16, 2023.

INTRODUCTION

In this era of continuously evolving technology, remote monitoring has emerged as an innovative and effective solution for monitoring and managing remote areas. Remote areas are often characterized by limited accessibility or physical constraints, and the utilization of remote monitoring technology plays a pivotal role in acquiring real-time data and enabling efficient remote monitoring from a distance [1], [2]. Several sectors where remote monitoring could benefit include Water Gate Monitoring [3], Weather Base Station [4], Sea Level Monitoring [5], and large-scale Solar Panel Monitoring [6]. The primary benefits of remote monitoring in such areas include enhanced efficiency and accuracy in monitoring and management, which can assist researchers or field personnel directly accessing data from inaccessible locations and to promptly identifying and monitoring threats [7].

Remote devices, including the Remote Terminal Unit (RTU), commonly employ non-rechargeable batteries. The RTU serves as a controller for remote monitoring and control operations [8]. In remote areas where a power source is absent, the RTU relies on battery power for its functionality. Thus, the implementation of a remote monitoring on non-rechargeable battery and a battery redundant system becomes crucial. These measures allow

field operators sufficient time to replace batteries while ensuring uninterrupted operation of the RTU device.

By implementing remote monitoring to the non-rechargeable battery components, field operators can manage battery usage through remote monitoring. This achieved by leveraging, the Internet of Things (IoT) and employing the Message Queuing Telemetry Transport (MQTT) communication protocol [9], [10]. The quality of data transmission is analyzed based on Quality of Service (QoS), considering parameters such as delay and packet loss [11]. As the loss of non-rechargeable battery power poses known threat to the functionality of these remote devices, a battery redundant system is regularly implemented to serve as a second power supply [12].

This paper highlights two preceding studies that reflect similar usage and circumstances of the current study [12], [13]. These precursor systems [12], [13] utilize two microcontrollers (Arduino and Wemos) to monitor and transmit data through the MQTT communication protocol respectively. The MQTT communication protocol is connected to a Node-RED interface where the monitored data are presented. In addition, the two preceding studies have two distinct battery redundant systems and goals. One study focused on the development of an Uninterruptible Power Supply (UPS) monitoring system that aims to ensure continuous power supply and monitor the performance of the UPS device [13], while the other monitors the power switching and notifies when the backup power generator is utilized instead of the main power supply [12].

The previous study [12] had some limitations, including the absence of sensor calibration testing for the ACS current and voltage sensors, as well as the lack of analysis on network quality such as delay and packet loss. Similarly, in another study [13], the system design merely involved a simulation using a potentiometer as a voltage and current sensor for monitoring the UPS device. The circuit design was implemented on a breadboard and lacked a mechanical casing design for the monitoring circuit. Additionally, the interface display in Node-RED was relatively simple. Moreover, the monitoring of multiple devices was limited to only two simulated devices.

Acknowledging the aforementioned, this study proposes an improved system in multiple devices remote monitoring, battery redundant, and communication from previous studies [12], [13] to be applied to multiple-device monitoring of non-rechargeable batteries. The new design proposed in this study is utilizes one microcontroller (Wemos D1 Mini) for each devices to improve working efficiency. The data received by the microcontroller are transmitted to the Node-RED interface through MQTT communication protocol. On that note, this study adds the concept of multiple device communication (multipoint-to-point) to a Node-RED interface is possible through MQTT communication protocol. This study also proposes the usage of a novel battery redundant system that is capable to manage battery switching using a Bootstrap High-Side circuit. To summarize, the aim of this study is to improve the working efficiency of remote monitoring systems, introduce the concept of multiple device monitoring on one interface, and develop a novel non-rechargeable battery redundant system.

METHOD

General Design System

This study focuses on the monitoring of battery current usage, battery voltage, and power consumption, as well as the battery box environment, including temperature and humidity, implemented for long-distance monitoring of non-rechargeable batteries. For this purpose, INA219 and DHT11 sensors were used to obtain the aforementioned data respectively. These accumulated data are then taken by the Wemos D1 Mini [14] microcontroller and presented

on a Node-RED interface [15] through the MQTT broker using the Message Queuing Telemetry Transport (MQTT) communication protocol.

This study also introduces a novel battery redundant system that uses a Bootstrap High-Side circuit to remove concerns of power loss and memory loss during power supply switching. To indicate this, the battery pack was tested by employing an RTU simulation. The RTU simulation consists of an Arduino UNO microcontroller running a LED program that uses the monitored battery as a power supply. The block diagram of the system is shown in Figure 1.

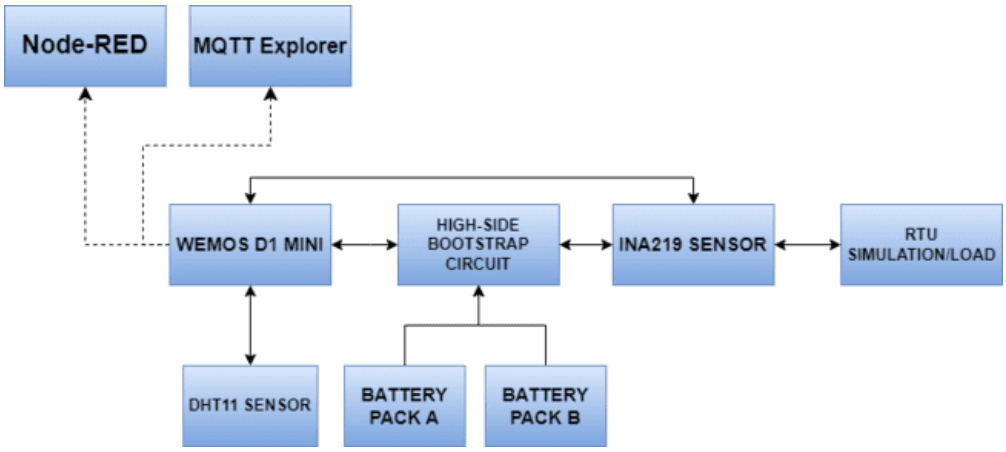

Figure 1. Block Diagram of the System

Mechanical Design System

The mechanical system houses a controller box, Remote Terminal Unit (RTU) simulation box, battery pack box, and acrylic base (Figure 2). Controller box contains a Wemos D1 Mini microcontroller, INA219 sensor, and bootstrap high-side circuit. The battery pack box has two battery packs (A and B), and the RTU simulation box was used to store the RTU simulation.

The main components of the mechanical system design are described in the following sections, as illustrated in Figure 2. Dimensions: Acrylic Base, 320 x 280 x 5 mm; Controller Box, 185 x 115 x 60 mm; Battery Pack Box, 150 x 95 x 50 mm; RTU Simulation Box, 125 85 x 50 mm.

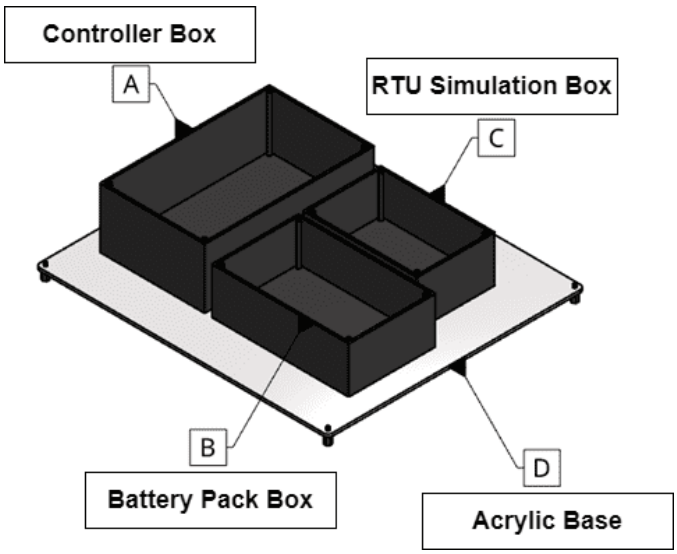

Figure 2. Layout Design of the Mechanical System

Electrical Design System

The Wemos D1 Mini microcontroller is equipped with an ESP8266 module to execute programs (non-rechargeable battery redundant system monitoring) and transmit sensor data. Figure 3 shows the electrical wiring of the system.

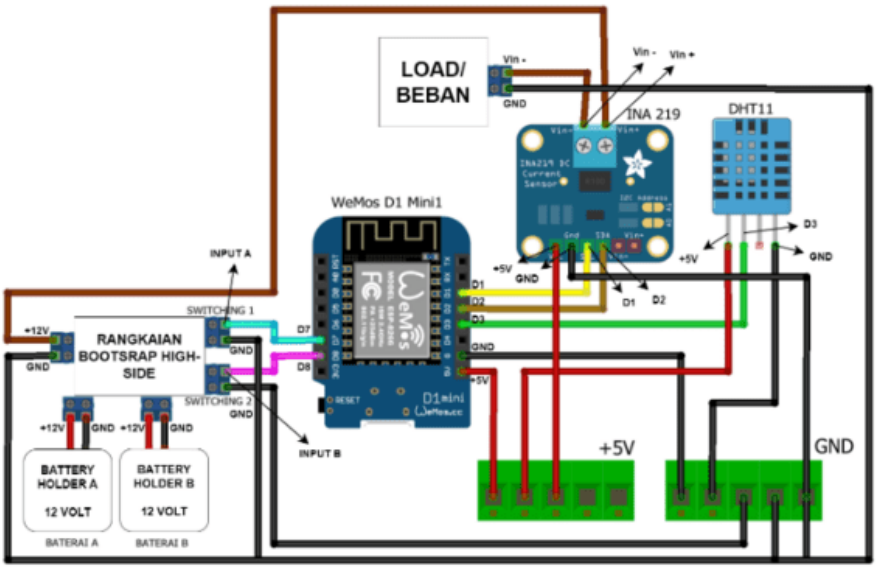

Figure 3. Wiring Design of the Electrical System (Device 1-4)

Additionally, a High-Side Bootstrap circuit schematic is shown in Figure 4. This circuit is utilized for battery redundant system.

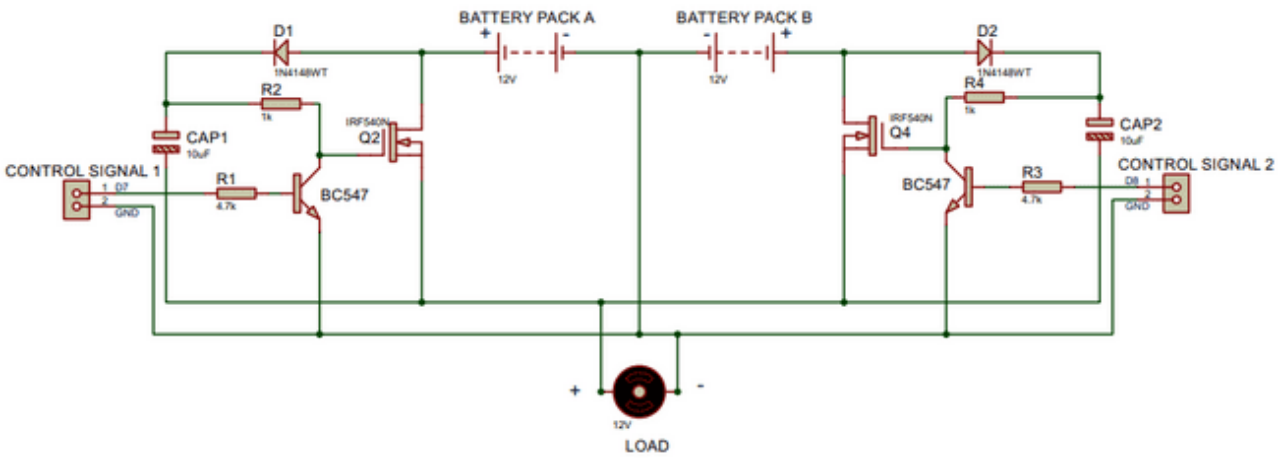

Figure 4. High-Side Bootstrap Circuit Schematic

Software Design System

Simultaneously, the Wemos D1 microcontroller uses the data from the INA219 sensor to monitor the current usage, battery voltage and power consumption of the battery, the Wemos D1 Mini microcontroller is able to release commands to switch from one main power supply to another. To simulate this, two AA battery packs (A and B) are used, each capable of producing 12V. The control command applied is switching when the battery pack has reached a voltage of less than 10 Volts. To determine which battery pack will be used, a High-Side Bootstrap circuit was utilized. Simultaneously, the High-Side Bootstrap can also remove the concern of power loss and memory loss between power supply switches.

To indicate that there was no power or memory loss, the battery pack is tested by a Remote Terminal Unit (RTU) simulation. This RTU consists of an Arduino UNO

microcontroller and a running LED program. On that note, the RTU simulation uses the battery packs (A and B) as a power supply and can determine that there is no power or memory loss if the LED program continues running during power supply switching controlled by the Wemos D1 microcontroller. A flowchart of the program is shown Figure 5.

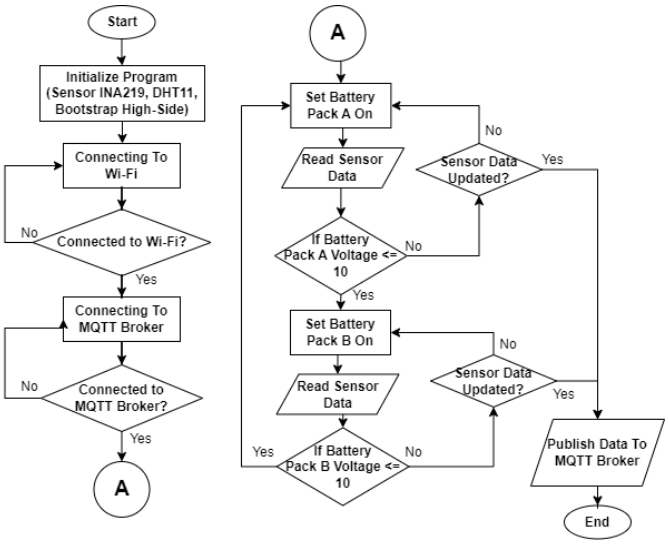

Figure 5. Microcontroller Program Flowchart

By utilizing the MQTT communication protocol, each microcontroller transmits data to the MQTT broker (Mosquitto Broker). The data received by the MQTT broker can be monitored using MQTT Explorer. The design model of the communication system is illustrated in Figure 6.

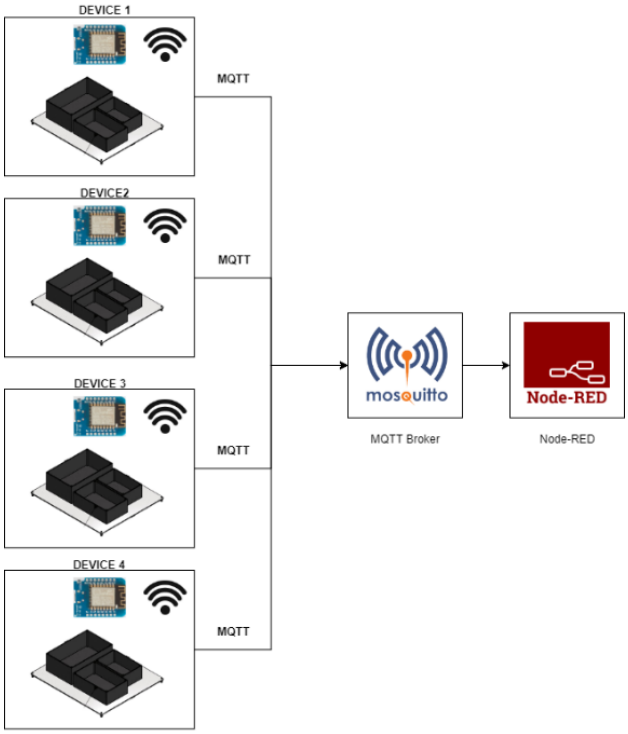

Figure 6. Design Model of the Communication

Node-RED was utilized to monitor all devices. The interface appearance on the Node-RED shows the data reading from battery voltage, current load, power load, temperature, humidity,

and battery pack usage status. An illustration of the interface design of the Node-RED is shown in Figure 7.

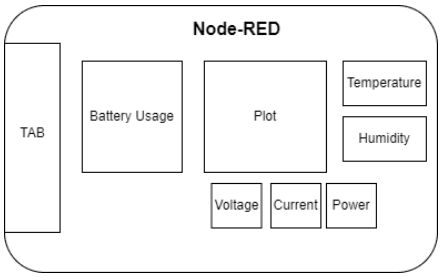

Figure 7. Node-RED Interface Illustration

System Design Testing

In this step, the overall system is analyzed. These systems will be tested to measure the error value of INA219 sensor, QoS (delay and packet loss) based on TIPHON standard, and the success rate of redundant system.

To obtain the percentage error value, the INA219 sensor reading value was compared with the measured value using a digital multimeter. The error percentage measurement is calculated using equation (1) [16].

$$error\ (\%) = \frac{measured\ value - reading\ value}{measured\ value} \times 100\ \% \quad (1)$$

where the measured value is obtained by measuring with a digital multimeter, and the reading value is indicated on the microcontroller.

Quality of service (QoS) is a method to measure the performance of a network and its service properties. QoS can assist users in observing the network-based application performance. The measurements for QoS use two parameters, delay and packet loss, based on the TIPHON standard using Wireshark Software[11], [17]. Delay is calculated using equation (2) and packet loss is calculated using equation (4)

$$Delay\ = delay\ 2 - delay\ 1 \quad (2)$$

$$Delay\ Average = \frac{\sum delay}{total\ packet} \quad (3)$$

Where,

Delay 1 = first transmission delay
Delay 2 = second transmission delay
$\sum delay$= delay difference amount

$$packet\ loss\ (\%) = \frac{packet\ sent - packet\ received}{packet\ sent} \times 100\ \% \quad (4)$$

Where,

Packet sent = amount of packet volume sent
Packet received = amount of packets successfully received

Table 1 and Table 2 shows the standard delay and packet loss according to TIPHON.

Table 1. Delay Based on TIPHON Standard

Delay Category	Delay (ms)	Index
Excellent	<150	4
Good	150-300	3

Fair	300-450	2
Bad	>450	1

Table 2. Packet Loss Based on TIPHON standard

Delay Category	Packet Loss (%)	Index
Excellent	<150	4
Good	150-300	3
Fair	300-450	2
Bad	>450	1

Redundant system testing was performed for this study by applying a High-Side Bootstrap into two 12 Volts AA battery packs as a power supply. The success rate of the redundant system is measured when battery pack A has reached 10 Volts, and it automatically switches to battery pack B. Additionally, functionality testing is performed for the High-Side Bootstrap. The calculation analysis is as follows. Equations (5) and (6) calculate of the percentage of successful input and output supply requirements for high-side bootstrap circuits.

$$Input\ Supply\ Requirements = \frac{Input}{12\ V} \times 100\ \% \quad (5)$$

$$Output\ Supply\ Requirements = \frac{Output}{12\ V} \times 100\ \% \quad (6)$$

Where,

Input = input voltage of High-Side Bootstrap Circuit

Output = output voltage of High-Side Bootstrap Circuit

RESULT AND DISCUSSION

Mechanical Design Results

During the mechanical design testing, several layout adjustments were made to the boxes of all devices to ensure ease of operation. Each device is equipped with identical electrical wiring, as depicted in Figure 8. The layout adjustment results are shown in Figure 9.

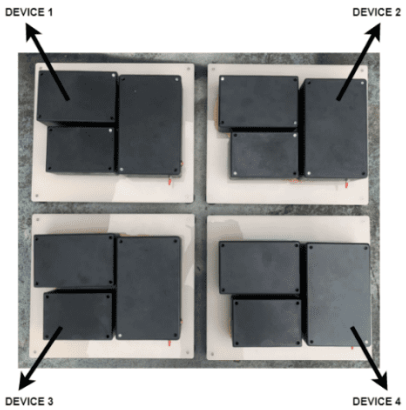

Figure 9. Layout Result of Mechanical Design (Device 1-4)

Electrical Design Results

Within the electrical design, there are several tests including the wiring of the Wemos D1 Mini. The electrical wiring results for the devices are shown in Figure 9. Additionally, functionality testing was performed using the High-Side Bootstrap circuit. Figure 10 shows

the result of Bootstrap High-Side Circuit wiring and Table 3 presents the results of the input and output efficiency of the High-Side Bootstrap circuit.

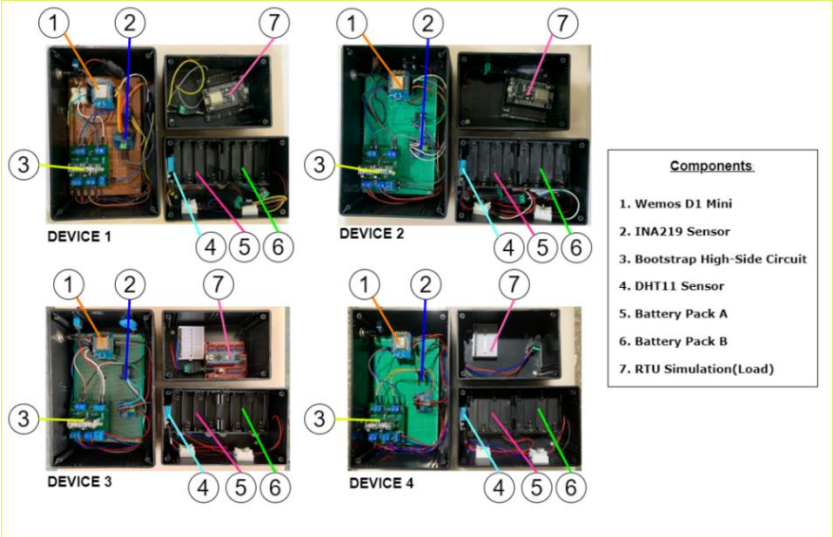

Figure 10. Result of the Electrical Wiring (Device 1-4)

Figure 11. Result of the Bootstrap High-Side Circuit Wiring (Device 1-4)

Among all the devices, there is a dedicated Bootstrap High-Side circuit (Figure 12) in each device that functions to control the utilization of the battery pack. The circuit requires 12 V input and 12 V output, which aligns with the used battery. Consequently, an efficiency evaluation of the circuit was performed, resulting in Table 3.

Table 3. High-Side Bootstrap Circuit Efficiency Testing Results

Circuit	Supply Requirements	I/O	Voltage	Success Rate
1	12 V	Input	11,8 V	98,3 %
		Output	11,4 V	95 %
2	12 V	Input	12 V	100 %
		Output	11,5 V	96,8 %
3	12 V	Input	12 V	100 %
		Output	11,5 V	96,8 %
4	12 V	Input	11,9 V	99,1 %
		Output	11,4 V	95 %

Bootstrap High-Side circuit efficiency test results average from all devices are 99.35% for input and 95.9% for output. Despite the presence of a voltage drop at the output owing the

working voltage of the electronic components, all of the High-Side Bootstrap circuit continues to operate with a success percentage exceeding 90% for both input and output.

Software Design Results

Software design tests were performed on the microcontroller program flow in transmitting data to the MQTT broker and the Node-RED interface.

MQTT communication between the system and MQTT Mosquitto broker was successful, as confirmed by the reception and display of data in the MQTT Explorer software. The received data include the temperature, humidity, voltage, current, power, and battery usage status. Figure 13 is a display of data received in MQTT Explorer

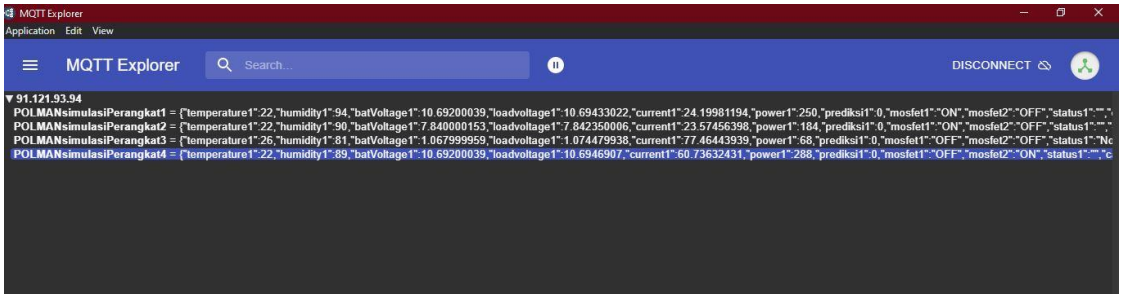

Figure 13. MQTT Explorer Data Display

The data obtained from the MQTT broker are effectively integrated into the Node-RED interface, allowing for the visualization and presentation of essential parameters such as temperature, humidity, voltage, current, power, and battery usage status. Figure 14 shows the result of the Node-RED interface

Figure 14. Node-RED Interface Result

System Design Testing Results

The INA219 sensor was measured ten times for each device, and the results were compared to a digital multimeter as a reference. 12V/1A adapter was used as the power supply.

The results show that Device 1 (Table 4) obtained a voltage error value of 0% - 1.6% and the current error value of 0.9% - 2.7%. The average error values of the voltage and current in Device 1 were 0.80% and 1.76%.

Table 4. Device 1 INA210 Voltage and Current Error Value

Test-	Device 1					
	V sensor (V)	V real (V)	V Error (%)	I sensor (mA)	I measured (mA)	I Error (%)
1	12,2	12,2	0	114	112	1,7
2	12,0	12,2	1,6	111	113	1,7
3	12,1	12,1	0	112	113	0.9
4	12,3	12,1	1,6	113	110	2,7
5	12,0	12,2	1,6	113	110	2,7
6	12,0	12,2	1,6	115	113	1,7
Test-	Device 1					
	V sensor (V)	V real (V)	V Error (%)	I sensor (mA)	I measured (mA)	I Error (%)
7	12,1	12,1	0	113	110	2,7
8	12,1	12,1	0	114	112	1,7
9	12,0	12,2	1,6	112	111	0,9
10	12,2	12,1	0,8	109	110	0,9

The results showed that Device 2 (Table 5) obtained a voltage error value of 0% - 1.6% and a current error value of 1.7% - 5.4%. The average error value of voltage and current in Device 2 are 0.88% and 2.45%.

Table 5. Device 2 INA219 Voltage and Current Error Value

Test-	Device 2					
	V sensor (V)	V real (V)	V Error (%)	I sensor (mA)	I measured (mA)	I Error (%)
1	12,0	12,2	1,6	116	110	5,4
2	12,0	12,1	0,8	110	112	1,7
3	12,1	12,2	0,8	110	111	1,9
4	12,1	12,2	0,8	111	110	0,9
5	12,2	12,2	0	112	110	1,7
6	11,9	12,1	1,6	107	110	6,0
7	12,2	12,2	0	109	112	2,6
8	12,0	12,2	1,6	110	112	1,7
9	12,1	12,2	0,8	110	111	0,9
10	12,0	12,1	0,8	112	110	1,7

The results showed that Device 3 (Table 6) obtained a voltage error value of 0% - 1.6% and the current error value of 0% - 3.6%. The average error value of voltage and current in Device 3 are 0.64% and 2.07%.

Lastly, the results showed that Device 4 (Table 7) obtained a voltage error value of 0% - 2.4% and the current error value of 0% - 2.7%. The average error value of voltage and current in device 4 are 1.04% and 1.17%, respectively.

In comparison to the preceding study, the implementation of INA219 in measuring the voltage and current demonstrated average error values of 0.29% and 2.29% respectively. These findings indicated that the error values obtained were comparable to those reported in a previous study[18].

According to these results, the error values of INA219 sensor readings are within the tolerable limit of less than 5%. Errors that occur are caused by the quality of the sensors.

Table 6. Device 3 INA219 Voltage and Current Error Value

Test-	Device 3					
	V sensor (V)	V real (V)	V Error (%)	I sensor (mA)	I measured (mA)	I Error (%)
1	12,0	12,2	1,6	114	110	3,6
2	12,1	12,2	0,8	114	111	2,7
3	12,2	12,2	0	113	110	2,7
4	12,0	12,1	0,8	114	110	3,6
5	12,0	12,1	0,8	114	110	3,6
6	12,2	12,2	0	112	110	1,8
7	12,2	12,1	0,8	112	111	0,9
8	12,0	12,2	0,8	113	112	0,9
9	12,1	12,2	0,8	111	111	0
10	12,1	12,1	0	111	112	0,9

Table 7. Device 4 INA219 Voltage and Current Error Value

Test-	Device 4					
	V sensor (V)	V real (V)	V Error (%)	I sensor (mA)	I measured (mA)	I Error (%)
1	12,0	12,2	1,6	114	110	3,6
2	12,1	12,2	0,8	114	111	2,7
3	12,2	12,2	0	113	110	2,7
4	12,0	12,1	0,8	114	110	3,6
5	12,0	12,1	0,8	114	110	3,6
6	12,2	12,2	0	112	110	1,8
7	12,2	12,1	0,8	112	111	0,9
8	12,0	12,2	0,8	113	112	0,9
9	12,1	12,2	0,8	111	111	0
10	12,1	12,1	0	111	112	0,9

Quality of Service (QoS) Result

The results of the Quality of Service testing for measuring two parameters, namely delay and packet loss, are presented in Table 8. The testing was conducted using a personal hotspot with XL Axiata SIM cards, where each device was connected to the same Internet network. The distances between Device 1, 2, 3, and 4 from Internet source were 2, 4, 6, and 8 m, respectively.

The average delay for Device 1 was 40.9 ms. In terms of Device 2, the average delay was 119.7 ms. For Device 3, the average delay recorded was 72.9 ms. Lastly, Device 4 exhibited an average delay of 99.8 ms. Based on the TIPHON standard, Devices 1, 2, 3, and 4 fall into the category of "Excellent." The average packet loss for Devices 1, 2, 3, and 4 is 0%. According to the TIPHON standard, all four devices fall into the "Excellent" category.

In contrast to earlier studies, the utilization of MQTT for monitoring systems yielded an average delay value of 41.91 ms, while achieving a packet loss rate of 0% [19]. The distance between the devices and the Internet source, as well as the quality of the Internet provider and MQTT broker, can influence the delay during testing. The farther the devices from the

Internet source, the poorer the Internet quality becomes, resulting in delays in the transmission of data from devices to the MQTT broker.

Table 8. Quality of Service (QoS) Delay and Packet Loss Measurement

Test	Device 1 (2 meter)		Device 2 (4 meters)		Device 3 (6 meters)		Device 4 (8 meters)	
	Delay (ms)	Packet Loss (%)	Delay (ms)	Packet Loss (%)	Delay (ms)	Packet Loss (%)	Delay (ms)	Packet Loss (%)
1	30,1	0	26,9	0	41,7	0	293,0	0
2	70,2	0	134,8	0	25,7	0	90,8	0
3	92,8	0	43,5	0	19,2	0	124,0	0
4	30,3	0	125,1	0	106,5	0	16,8	0
5	39,2	0	72,3	0	111,8	0	139,6	0
6	42,0	0	53,6	0	70,3	0	274,0	0
7	38,9	0	92,8	0	69,1	0	180,1	0
8	30,8	0	121,7	0	130,5	0	39,4	0
9	12,8	0	215,9	0	135,6	0	10,8	0
10	22,6	0	112,2	0	18,6	0	29,0	0

Redundant System Result

Redundant system testing was conducted five times for each device. The testing involved the transfer of battery packs A to B, battery packs B to A, and the RTU simulation conditions using a bootstrap high-side circuit. Table 9 presents the testing results of the redundant system for Device 1 and Device 2, while Table 10 displays the testing outcomes for the redundant system of Device 3 and Device 4.

Table 9. Device 1 and Device 2 Redundant System Testing Results

Test-	Device 1				Device 2			
	A - B	Load Condition	B - A	Load Condition	A - B	Load Condition	B - A	Load Condition
1	✓	On	✓	On	✓	On	✓	On
2	✓	On	✓	On	✓	On	✓	On
3	✓	On	✓	On	✓	On	✓	On
4	✓	On	✓	On	✓	On	✓	On
5	✓	On	✓	On	✓	On	✓	On

Table 10. Device 3 and Device 4 Redundant System Testing Results

Test-	Device 3				Device 4			
	A - B	Load Condition	B - A	Load Condition	A - B	Load Condition	B - A	Load Condition
1	✓	On	✓	On	✓	On	✓	On
2	✓	On	✓	On	✓	On	✓	On
3	✓	On	✓	On	✓	On	✓	On
4	✓	On	✓	On	✓	On	✓	On
5	✓	On	✓	On	✓	On	✓	On

The redundant system testing on RTU simulation for Device 1 achieved a success rate of 100%. Device 2 also achieved a success rate of 100%. Similarly, Device 3 and Device 4 both

obtained a success rate of 100% in the testing. The bootstrap high-side circuit designed to control the battery package usage in each device successfully functioned as intended, despite experiencing a voltage drop in its output during circuit testing.

According to previous investigations, the incorporation of a redundant system in solar photovoltaic setups results in an average power interruption duration of approximately 2.79 to 3.07 seconds from the onset of switching until the load is successfully restored [20].

CONCLUSION AND FUTURE WORK

Based on the discussion of this study, it can be concluded that the Design of a Remote Monitoring Application on Non-Rechargeable Battery Redundant System has been completed by simulating a similar concept to the actual plant (RTU). The study results indicate that the INA219 sensor shows an average error of 0.64% - 1.04% for voltage and 1.17% - 2.45% for current. Quality of Service testing reveals an average delay of 40.9 - 119.7 ms with 0% packet loss, meeting the excellent standard. Bootstrap High-Side circuit efficiency percentage average from all devices are 99.35% for input and 95.9% for output. Lastly, the redundant system tests achieve a 100% success rate on all devices, confirming the successful design implementation.

For future studies, it is recommended to utilize real plants instead of prototypes to obtain more diverse and realistic data. Furthermore, eliminating the reliance on an internet connection would be beneficial for achieving long-range monitoring without internet network dependencies. Developing smaller devices that can be easily deployed as plug-and-play solutions is also advisable for enhanced convenience and practicality.

REFERENCES

[1] F. Capraro, S. Tosetti, F. Rossomando, V. Mut, and F. Vita Serman, "Web-based system for the remote monitoring and management of precision irrigation: A case study in an arid region of Argentina," *Sensors*, vol. 18, no. 11, p. 3847, 2018, doi: 10.3390/s18113847.

[2] P. S. Priambodo, W. Purnomo, A. Subiantoro, A. Muis, and F. Yusivar, "Transformerless high voltage and controllable current battery charger for e-car," presented at the 2013 Joint International Conference on Rural Information & Communication Technology and Electric-Vehicle Technology (rICT & ICeV-T), IEEE, 2013, pp. 1–4. doi: 10.1109/rICT-ICeVT.2013.6741492.

[3] W. Sanjula, K. Kavinda, M. Malintha, W. Wijesuriya, S. Lokuliyana, and R. de Silva, "Automated water-gate controlling system for Paddy fields," presented at the 2020 2nd International Conference on Advancements in Computing (ICAC), IEEE, 2020, pp. 61–66. doi: 10.1109/ICAC51239.2020.9357312.

[4] S. Aminah, A. D. Mulyadi, and Y. Erdani, "The Wireless Acquisition Data System Simulator Design on Automatic Weather Monitoring Station," *Motiv. J. Mech. Electr. Ind. Eng.*, vol. 1, no. 3, Art. no. 3, Sep. 2019, doi: 10.46574/motivection.v1i3.33.

[5] F. Amaluddin and A. Haryoko, "Analisa Sensor Suhu Dan Tekanan Udara Terhadap Ketinggian Air Laut Berbasis Mikrokontroler," *Antivirus J. Ilm. Tek. Inform.*, vol. 13, no. 2, pp. 98–104, 2019, doi: 10.35457/antivirus.v13i2.843.

[6] S. Shapsough, M. Takrouri, R. Dhaouadi, and I. Zualkernan, "An MQTT-Based Scalable Architecture for Remote Monitoring and Control of Large-Scale Solar Photovoltaic Systems," in *Smart Grid and Internet of Things*, A.-S. K. Pathan, Z. Md. Fadlullah, and M. Guerroumi, Eds., in Lecture Notes of the Institute for Computer Sciences, Social Informatics and Telecommunications Engineering. Cham: Springer International Publishing, 2019, pp. 57–67. doi: 10.1007/978-3-030-05928-6_6.

[7] N. Poma *et al.*, "Remote monitoring of seawater temperature and pH by low cost sensors," *Microchem. J.*, vol. 148, pp. 248–252, 2019, doi: 10.1016/j.microc.2019.05.001.
[8] F. Salahudin and B. Setiyono, "Design of Remote Terminal Unit (RTU) Panel Supply Monitoring Based on IOT Case Study at PLN," presented at the 2019 6th International Conference on Information Technology, Computer and Electrical Engineering (ICITACEE), IEEE, 2019, pp. 1–6.
[9] Z. B. Abilovani, W. Yahya, and F. A. Bakhtiar, "Implementasi Protokol MQTT Untuk Sistem Monitoring Perangkat IoT," *J. Pengemb. Teknol. Inf. Dan Ilmu Komput. E-ISSN*, pp. 7521–7527, 2018.
[10] P. Anggraeni, W. A. Candra, M. Defoort, and M. Djemai, "Experimental implementation of fixed-time leader-follower axial alignment tracking," presented at the 2019 International Conference on Mechatronics, Robotics and Systems Engineering (MoRSE), IEEE, 2019, pp. 86–91. doi: 10.1109/MoRSE48060.2019.8998638.
[11] V. Barot, V. Kapadia, and S. Pandya, "QoS enabled IoT based low cost air quality monitoring system with power consumption optimization," *Cybern. Inf. Technol.*, vol. 20, no. 2, pp. 122–140, 2020, doi: 10.2478/cait-2020-0021.
[12] A. A. Mukhlisin, S. Suhanto, and L. S. Moonlight, "Rancang Bangun Kontrol Dan Monitoring Baterai Uninterruptible Power Supply (Ups) Menggunakan Energi Hybrid Dengan Konsep Internet Of Thing (IOT)," presented at the Prosiding SNITP (Seminar Nasional Inovasi Teknologi Penerbangan), 2019.
[13] M. U. Mehmood, W. Ali, A. Ulasyar, H. S. Zad, A. Khattak, and K. Imran, "A Low Cost Internet of Things (LCIoT) Based System for Monitoring and Control of UPS System using Node-Red, CloudMQTT and IBM Bluemix," presented at the 2019 International Conference on Electrical, Communication, and Computer Engineering (ICECCE), IEEE, 2019, pp. 1–5. doi: 10.1109/ICECCE47252.2019.8940686.
[14] F. Suryatini, W. Purnomo, and R. R. Harlanti, "Sistem kendali penyemaian bersusun pada tanaman hidroponik berbasis logika fuzzy Tsukamoto dengan aplikasi Blynk: A tiered seeding control system for hydroponic plants based on Tsukamoto's fuzzy logic with the Blynk application," *JITEL J. Ilm. Telekomun. Elektron. Dan List. Tenaga*, vol. 3, no. 1, pp. 37–46, 2023, doi: 10.35313/jitel.v3.i1.2023.37-46.
[15] A. Jothivelu and S. P. Simon, "A Smart BTS/Node B Network Monitoring and Control using IoT," presented at the 2019 Fifteenth International Conference on Information Processing (ICINPRO), IEEE, 2019, pp. 1–5. doi: 10.1109/ICInPro47689.2019.9092317.
[16] W. A. Candra, A. S. Sunarya, and W. S. Saraswati, "Computer Vision Implementation in Scratch Inspection and Color Detection on The Car Roof Surface," *Motiv. J. Mech. Electr. Ind. Eng.*, vol. 5, no. 2, Art. no. 2, Apr. 2023, doi: 10.46574/motivection.v5i2.230.
[17] R. Subektiningsih and P. Ferdiansyah, "Analisis Perbandingan Parameter QoS Standar TIPHON Pada Jaringan Nirkabel Dalam Penerapan Metode PCQ," *Explore*, vol. 12, no. 1, pp. 57–63, 2022, doi: 10.35200/explore.v12i1.527.
[18] M. Mungkin, H. Satria, J. Yanti, G. B. A. Turnip, and S. Suwarno, "Perancangan Sistem Pemantauan Panel Surya Pollycristalline Menggunakan Teknologi Web Firebase Berbasis IoT," *INTECOMS J. Inf. Technol. Comput. Sci.*, vol. 3, no. 2, pp. 319–327, Dec. 2020, doi: 10.31539/intecoms.v3i2.1861.
[19] S. Pramono, S. Indriyanto, and W. Junianto, "The Implementation of MQTT Protocol using PT-100 for Monitoring the Vaccine Temperature," *J. RESTI Rekayasa Sist. Dan Teknol. Inf.*, vol. 6, pp. 346–351, Apr. 2022, doi: 10.29207/resti.v6i2.3988.
[20] Y. Mahaseng, M. Masarrang, Y. Arifin, M. Mustofa, and S. Dewi, "RANCANG BANGUN PANEL AUTOMATIC TRANSFER SWITCH (ATS) BERBASIS PHOTOVOLTAIC," *Foristek*, vol. 12, no. 1, Art. no. 1, Jun. 2022, doi: 10.54757/fs.v12i1.140.